THE ASTROPHYSICAL JOURNAL, 348:503–514, 1990 January 10

CO $J = 3$–2 OBSERVATIONS OF THE NEUTRAL DISK IN SAGITTARIUS A WEST

E. C. SUTTON, W. C. DANCHI, AND P. A. JAMINET
Department of Physics and Space Sciences Laboratory, University of California, Berkeley

AND

C. R. MASSON
Department of Physics, California Institute of Technology
Received 1989 March 1; accepted 1989 July 7

ABSTRACT

We have studied the distribution of CO $J = 3$–2 emission from the dense neutral disk in Sgr A West. The distribution observed is similar to that seen in the low-excitation CO $J = 1$–0 line but shows a stronger concentration toward the central higher excitation regions of the disk. The regions of strongest CO $J = 3$–2 emission correspond closely with those seen in high-excitation transitions such as CO $J = 7$–6 and HCN $J = 1$–0. The disk is highly clumped as may be seen from the strongly saturated behavior of the CO line intensities. Inferred CO column densities through individual clumps are as high as 2×10^{19} cm^{-2}, whereas typical beam-averaged column densities are more like 2×10^{18} cm^{-2}. The excitation implies gas kinetic temperatures in the range $T = 100$–200 K, somewhat lower than temperatures inferred from metastable NH_3 observations. Densities are found to range from 2×10^4 cm^{-3} up to at least 2×10^5 cm^{-3}, in good agreement with the densities derived from HCN and CS.

The kinematic structure shows gas in relatively simple circular motion about the center as well as substantial evidence for considerable noncircular motions. A number of well-delineated clouds have motions apparently unconnected with the dominant pattern of circular rotation. These clouds account for about 6% of the mass of the high-velocity gas. For that gas participating in circular rotation the rotation curve is found to be relatively flat between 2 and 8 pc. The mass enclosed within the central 2 pc radius is estimated to be $5.6 \times 10^6\ M_\odot$. The flat rotation curve implies a substantial distributed mass of $1.5 \times 10^7\ M_\odot$ between 2 and 8 pc.

Subject headings: galaxies: The Galaxy — galaxies: nuclei — interstellar: molecules

I. INTRODUCTION

The region around the Galactic center displays a great variety of phenomena across a wide range of spatial scales. On the 100 pc scale, the morphology of the region is best seen in radio continuum maps which are dominated by the nonthermal shell source Sgr A East, the central thermal region Sgr A West, and diffuse emission extending both out of the Galactic plane and in the Galactic plane toward positive Galactic longitudes. The component at positive longitude, variously referred to as the "Galactic center arc" or as the "spur" and "bridge" features, has been resolved into fascinatingly complex filamentary structures by Yusef-Zadeh, Morris, and Chance (1984). Immediately around Sgr A West is found a rotating disk of neutral gas, with an inner radius of 2 pc and an outer radius of about 8 pc. This disk is seen in a variety of molecular species, in atomic fine-structure lines, and also at infrared wavelengths through thermal dust emission (Becklin, Gatley, and Werner 1982). Inside the 2 pc inner radius of the neutral disk is a central ionized "cavity" in which the gas appears to be clumpy, but to be organized into coherent streamers. This streamer structure forms a three-element spiral-like feature which has been very well delineated by the radio continuum maps of Ekers *et al.* (1983) and Lo and Claussen (1983) and in the Ne II observations of Serabyn and Lacy (1985) and Serabyn, Güsten, and Evans (1988). On the smallest spatial scales observed there is the strong 2 μm source IRS 16 and the enigmatic compact nonthermal radio source Sgr A*. These and many other phenomena relating to the Galactic center region are more completely discussed in the comprehensive reviews of Oort (1977), Brown and Liszt (1984), and Genzel and Townes (1987).

Concentrating on the neutral disk, one of the best views of the distribution of molecular material in this region comes from the work of Serabyn *et al.* (1986). These authors mapped the distribution of the CO $J = 1$–0 emission in a $6' \times 2'$ region around Sgr A* at a spatial resolution of 21″. The low-velocity parts of the spectra were largely contaminated by molecular material distributed along the line of sight to the Galactic center. The higher velocity CO emission, however, was not similarly affected. In addition to CO these authors observed emission from CS $J = 2$–1 from a number of positions, in order to obtain information about the higher density regions of the disk. The kinematic picture obtained is one of a disk with a rotation axis inclined 65°–70° with respect to the line of sight. The rotational velocity of the disk is about 110 km s^{-1} and is nearly independent of radius from 3 pc out to 8 pc. The mass enclosed within the 2 pc inner radius was found to be about $6 \times 10^6\ M_\odot$.

In contrast, Harris *et al.* (1985) studied emission from the Galactic center in the $J = 7$–6 transition of CO, albeit with somewhat lower resolution (32″) and lower sensitivity and at a limited number of positions. In this higher excitation line they observed almost exclusively emission from the high-velocity gas in the dense neutral disk region. Combining their data with lower and higher J observations they concluded that the emission was from a region with a molecular hydrogen density of about 3×10^4 cm^{-3}, a gas temperature of about 300 K, and a beam-averaged column density of about 2×10^{18} cm^{-2}. All of

these values had fairly large uncertainties. They also saw a significant variation in rotational velocity with radius. From the kinematics of the central region, they derived a mass within the central 2 pc radius of $5 \times 10^6 M_\odot$. However, the kinematic picture was not simple, and substantial noncircular motions seemed to be present.

Other molecular observations have helped improve our view of this region. In particular we note the important HCN aperture synthesis measurements of Güsten *et al.* (1987) and the more recent HCO^+ and $H^{13}CN$ interferometric observations of Wright, Marr, and Backer (1988). With a resolution of about 10″, these observations show that the molecular emission forms an almost complete, symmetric ring. The material is clumpy, with densities of around 10^5 cm^{-3} in the clumps needed for collisional excitation.

In this work we have mapped a region of about 6′ × 3′ around Sgr A* in the $J = 3$–2 transition of CO. Our motivation was to obtain a picture of the molecular gas which was intermediate between and complementary to the pictures formed from the $J = 1$–0 and $J = 7$–6 observations. In the $J = 3$–2 transition the excitation requirements are sufficiently different than in $J = 1$–0 that the problem of foreground contamination in the low-velocity regions of the spectrum should be somewhat alleviated. Compared to the $J = 1$–0 data the $J = 3$–2 data should show a greater proportion of high-velocity emission, due to the enhanced density in the neutral disk. The availability of a new submillimeter telescope and a high-sensitivity receiver system operating at the 345 GHz frequency of the $J = 3$–2 line has allowed us to map this transition with both high spatial resolution (≈20″) and high sensitivity. It was possible for us to map an extensive region with a sensitivity and a spatial resolution comparable to that of the $J = 1$–0 observations of Serabyn *et al.* (1986). Like many other workers in this field, in what follows we adopt a "conventional" distance to the Galactic center of 10 kpc, so that an angular displacement of 1′ corresponds to a linear distance of 3 pc.

II. OBSERVATIONS

We obtained observations of the $J = 3$–2 line of CO in Sgr A West at the 10.4 m Caltech Submillimeter Observatory (CSO) during June of 1988. The receiver used was a 345 GHz SIS waveguide mixer receiver constructed at Berkeley (Sutton *et al.* 1989). The receiver exhibited its best noise performance of 275 K double sideband (DSB) at 312 GHz. At 345 GHz the receiver noise was typically 375 K (DSB). The backend was a 1024 channel 500 MHz acousto-optical spectrometer built for the CSO. Observations were obtained using the standard observatory procedures and software for telescope control, data acquisition, calibration, and data analysis. Atmospheric zenith opacities ranged from 0.15 to 0.35 during these measurements.

We mapped a grid of positions centered on the position of the compact radio source Sgr A*, $\alpha = 17^h42^m29^s.3$, $\delta = -28°59'18''.6$ (1950). The observations were spaced at intervals of 20″, representing very nearly full beamwidth spacing at this frequency. The orientation of the grid was aligned with the nominal Galactic reference frame, that is the grid positions were multiples of 20″ in the coordinates δl and δb. This is the same grid observed by Serabyn *et al.* (1986), and our positions correspond with theirs within the precision of the pointing. We estimate the pointing accuracy during our observations to have been 5″. In observing the CO $J = 1$–0 line Serabyn *et al.* measured a total of 127 positions on this grid, inside a 6′ × 4′ region in δl and δb. Our observations of CO $J = 3$–2 covered this region somewhat more thoroughly, with a total of 165 measured positions. The additional measured positions were mostly taken in a direction perpendicular to the plane of the molecular disk, which itself is tilted with respect to the nominal Galactic plane.

Each grid point was observed with 80 s of on-source integration time (except for the central position which was observed repeatedly and for which these repeated observations have been co-added). Position switching was employed, with off positions symmetrically offset by plus and minus 60′ in azimuth. All observations were made at times during the night when this switching was oriented in a direction which placed these reference positions well out of the Galactic plane.

Calibration was done using the chopper-wheel method in which the observations were scaled by ratioing to the spectrum of an ambient temperature load. Beam efficiencies were measured by observations of the Moon and Jupiter. All results quoted here have been corrected for the observed extended source (Moon) efficiency. The antenna temperatures shown should be multiplied by an additional factor of 1.9 in order to give main-beam brightness temperatures. The SIS receiver was operated in a double-sideband mode, and we have assumed in reducing the data that the sidebands were well balanced. Spot checks during the observations indicated that this was generally the case, although sideband imbalance may introduce calibration errors on the order of 10%. We believe our overall calibration to be good to within 30%.

Linear baselines were removed from all of the observed spectra. In a few cases a small quadratic component was also subtracted.

Due to some degradation at the edges of the passband, we have chosen to restrict our attention to a region in v_{lsr} ranging from −170 to 170 km s^{-1}. This range of velocities is known to include most velocities at which CO emission is seen toward the Galactic center, although some weak emission has been seen out to ±200 km s^{-1}. Within this range, three distinct types of features are present. At the most extreme velocities there is emission which has been associated with molecular material at distances out to about 1.5 kpc from the center (cf. Liszt and Burton 1978). At somewhat lower (but still rather high) velocities, one can see emission from the 2 pc radius dense rotating neutral disk. At still lower velocities, the most dominant features in the spectra are a series of deep absorptions produced by low-velocity foreground gas. All three of these regions will be discussed, although our emphasis will be on the emission from the dense neutral disk.

In Figure 1 we have presented spectra from a coarsely sampled subset of the positions which we have observed. The central spectrum, labeled ($\delta l = 0'$, $\delta b = 0'$), corresponds to the position of Sgr A*. The remaining spectra are offset in δl and δb by multiples of 1′ from Sgr A*. The spectrum at ($\delta l = 1'$, $\delta b = 0'$) is the closest of those shown to the peak of the lobe of redshifted emission from the dense neutral disk. The blue-shifted lobe is extended and is seen quite strongly in the spectrum at ($\delta l = 1'$, $\delta b = 0'$) and several others.

The foreground material is evident via absorption features at velocities of +15, −3, −31, and −53 km s^{-1}. Velocities of the absorption dips are quite constant thoughout the region mapped, confirming that they likely are produced in spatially extended clouds lying along the line of sight. The dip at −53 km s^{-1} has been identified as corresponding to material in the 3 kpc arm. The negative velocity features are all quite deep,

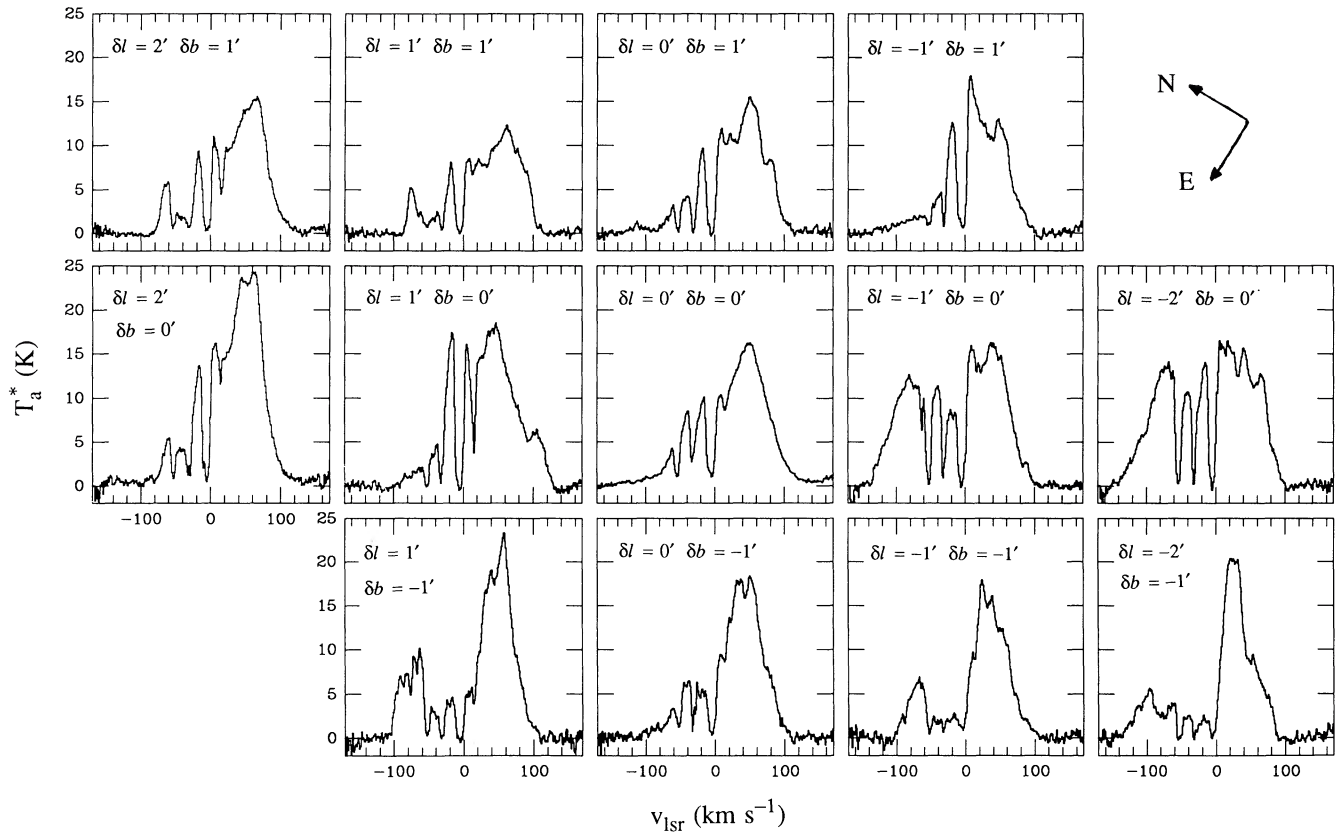

FIG. 1.—Spectra of CO $J = 3$–2 emission in the vicinity of the Galactic center. Positions given are offsets in Galactic coordinates from $\alpha = 17^h42^m29^s.3$, $\delta = -28°59'18''.6$ (1950), the assumed position of Sgr A*. The 13 spectra shown are a coarsely sampled subset of the 165 spectra obtained in this work.

generally extending down to near the level of the continuum, indicating a very high optical depth. The +15 km s^{-1} feature is not generally as deep and its strength varies across the map. It is possible that this "absorption" may represent variations in the emission from the spatially extended cloud at 20 km s^{-1}.

The highest velocity features evident in the data are very weak emission peaks at velocities of +165 and −135 km s^{-1}. In the model of Liszt and Burton (1978), the material contributing to this emission is thought to belong to a tilted, expanding and rotating disk extending out to a radius of 1.5 kpc from the center of the galaxy. Liszt and Burton (1980) substituted an explanation in which the gas motion in this region is along highly elliptical orbits, with no net expansion. Due to the limited spatial region mapped in our observations, we see this gas primarily at large absolute velocities. These features appear near the edges of our passband, and they are generally quite weak. However, such emission is clearly present in a number of spectra and is the reason the spectra often fail to drop back to the apparent continuum at the redshifted edge of the spectra.

Emission from the rotating neutral disk is very prominent in these spectra. The blueshifted emission peaks at a velocity of about −90 km s^{-1} and is strongest in a region centered about 1′.5 from Sgr A*, roughly $\delta l = -80''$, $\delta b = -20''$ in our coordinate grid. This emission is extended over a region of a few arcminutes. The redshifted emission at +90 km s^{-1} is located slightly closer to Sgr A*, is somewhat more compact, and is centered roughly at $\delta l = 60''$, $\delta b = 20''$. One observational problem slightly complicates the interpretation of the redshifted portion of the neutral disk emission. These observations were obtained with the receiver tuned in such a fashion that the frequency of the CS $J = 7$–6 line appeared in the opposite sideband from the CO $J = 3$–2 line. Such emission could contaminate the appearance of the CO spectra, but with the tuning employed this would only be possible for the redshifted portion of the spectrum and for redshifts of 90 km s^{-1} or greater. Fortunately the CS $J = 7$–6 line is hard to excite, requiring densities of about 10^6 cm^{-3} or greater. From the high-J CS observations of Serabyn, Güsten, and Evans (1988), we estimate that CS $J = 7$–6 would be observable only at those positions of the very highest density in the neutral ring, and that at such positions the contamination would be 1 K or less of main-beam brightness temperature.

Velocity channel maps of the data are presented in Figure 2. In these maps we have averaged the line intensity over ranges of either 10 or 15 km s^{-1}. Maps with $|v_{lsr}| \leq 60$ km s^{-1} are dominated by foreground absorption and spatially extended low-velocity emission. Prominent spatially extended clouds are the "20 km s^{-1}" cloud, which peaks at the southern (*lower right*) corner of the map, and the large "50 km s^{-1}" cloud, which peaks off the map on the eastern side (*lower left*). Maps near $|v_{lsr}| \approx 100$ km s^{-1} display the redshifted and blueshifted emission lobes of the rotating neutral disk. The redshifted lobe is compact and centered near ($\delta l = 1'$, $\delta b = 20''$). The blueshifted lobe near ($\delta l = -1'20''$, $\delta b = -20''$) is spatially extended and exhibits considerable internal structure. In particular we note that one boundary of this cloud is seen to be a ridge of strong emission along the line $\delta b = 0$, with a steep drop off in intensity at positive δb. Emission extends at least 2′ below this ridge. Besides these two features of the rotating neutral disk, there are additional molecular clouds clearly not

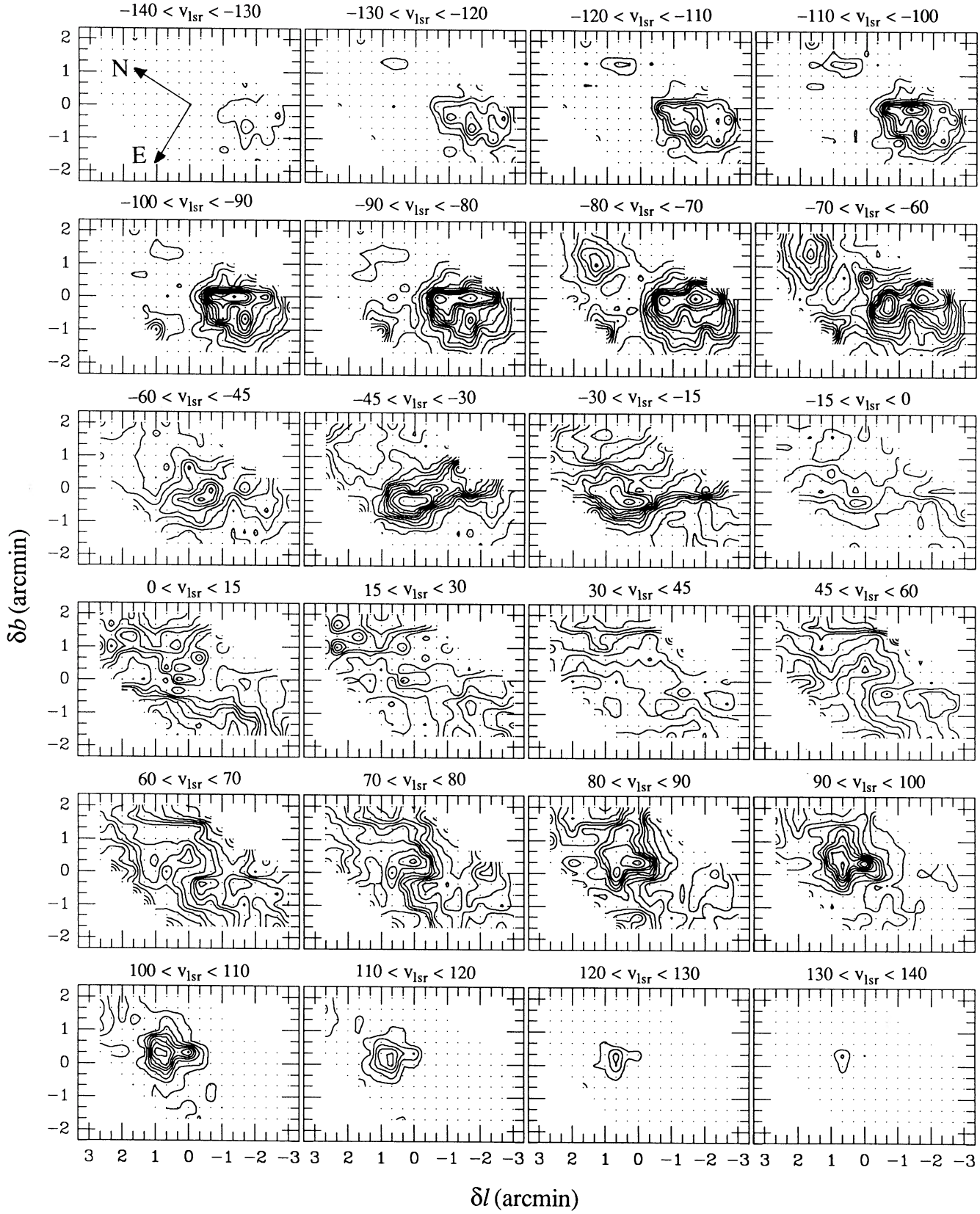

FIG. 2.—Velocity-averaged maps of CO $J = 3$–2 emission from Sgr A West. For $|v_{lsr}| > 60$ km s^{-1}, the averages are taken over 10 km s^{-1} bins; for $|v_{lsr}| < 60$ km s^{-1}, the bins are 15 km s^{-1} wide. In all maps the lowest contour level is 1 K with contours every 1 K through 10 K and every 2 K thereafter.

participating in circular rotation. One is an extended blue-shifted cloud at -70 km s^{-1} appearing at positive δl. Its direction of motion is contrary to the sense of rotation of the inner Galaxy. Another is an apparently compact cloud at -80 km s^{-1} centered at ($\delta l = 1'$, $\delta b = -1'$). A third is a clearly unresolved cloud at ($\delta l = 0'$, $\delta b = 40''$) with $v_{\rm lsr} = -65$ km s^{-1}. These last two clouds are rather near the presumed rotation axis of the neutral disk and hence also are not participating in simple rotation. It is interesting that all three of these clouds have similar velocities, although it is not clear that they are related in any other way.

III. RESULTS

a) Excitation Requirements

In analyzing the information present in the spatial distribution of molecular line emission, it is important to consider the factors affecting the strength of emission from various molecular species and in various transitions. The populations of molecular levels are determined by an equilibrium between radiative and collisional processes. Spontaneous emission measured by the Einstein A-coefficient varies greatly from transition to transition, being proportional to the square of the molecular dipole moment and the cube of the transition frequency. Collisional rates vary in a complex fashion from transition to transition but, broadly speaking, exhibit less variation than the spontaneous emission rate. Since collisional rates vary in proportion with the density of collisional partners (molecular hydrogen), there will be some density at which collisional and radiative rates are in balance. At higher densities, collisions are sufficiently frequent to maintain the gas in a state of thermal equilibrium. At lower densities, the spontaneous emission rate dominates and high lying levels have subthermal populations.

There are a variety of somewhat arbitrary methods which can be used to describe this balance. The simplest is to view the transition in question as a two-level system, in which case one can define a critical density, which we will call $n_{\rm cr1}$, as that at which the A-coefficient is just equal to the downward collisional rate:

$$A_{ul} = n_{\rm cr1}\,\gamma_{ul}\,.$$

In practice we are dealing with multilevel systems and transitions will be possible between a variety of levels. Restricting ourselves to linear molecules, spontaneous emission will still consist of a single transition from J to $J-1$. Collisions however will be possible from J to all allowed levels, both above and below. Equating the spontaneous emission rate with the sum of all collisional rates out of the level J (Hollenbach and McKee 1979) allows us to define a somewhat more appropriate critical density $n_{\rm cr2}$,

$$A_{J,J-1} = n_{\rm cr2} \sum_{J' \neq J} \gamma_{J,J'}\,.$$

Since this second definition includes more transitions than that in $n_{\rm cr1}$, it will always give a smaller numerical value for the critical density. This definition is still somewhat arbitrary since it is only a single parameter describing the balance of a large number of processes. In general one is most interested in knowing the equilibrium populations of all the various levels, information that can only be obtained by solving numerically the set of rate equations for all of the levels simultaneously. Critical densities for those transitions which are important to our discussion of Sgr A West are contained in Table 1. Details on the calculations and assumptions used in constructing this table are described in the Appendix.

TABLE 1

EXCITATION AND CRITICAL DENSITIES

Molecule	Transition	A-Coefficient (s^{-1})	$n_{\rm cr1}$(cm^{-3})	$n_{\rm cr2}$(cm^{-3})	β
CO	$J=1$–0	7.1(−8)	2.9(3)	2.7(2)	0.80
	2–1	6.9(−7)	1.5(4)	2.6(3)	0.45
	3–2	2.5(−6)	4.7(4)	9.2(3)	0.26
	7–6	3.4(−5)	6.4(5)	1.3(5)	0.15
CS	$J=2$–1	1.7(−5)	4.2(5)	6.4(4)	0.80
	3–2	6.1(−5)	1.4(6)	2.3(5)	0.65
	5–4	3.0(−4)	6.8(6)	1.2(6)	0.84
	7–6	8.4(−4)	2.0(7)	3.4(6)	0.99
HCN	$J=1$–0	2.4(−5)	4.5(6)	1.3(5)	0.54

This picture is not complete since we have ignored transitional rates associated with absorption and stimulated emission. This can include effects such as radiative pumping in which continuum radiation, due to thermal dust emission, plays a role in determining molecular excitation. Often the dominant effect is that of absorption of radiated photons by adjoining parts of a molecular cloud. In the escape probability formalism, this is described by a probability β that an emitted photon will escape the cloud before being reabsorbed. If the photon does not escape, this can be viewed as a reduction of the effective A-coefficient and a corresponding decrease in the critical density. Typical values for the escape probability are listed in Table 1, where for consistency we have adopted a kinetic temperature of 100 K (the highest temperature at which collisional rates for CS and HCN are available), a turbulent linewidth of 50 km s^{-1}, and a density of 10^5 cm^{-3}. For CO we have taken a column density of 10^{19} cm^{-2} and values of 10^{15} cm^{-2} for both CS and HCN. Details of this calculation are discussed more thoroughly in the Appendix. Escape probabilities significantly less than unity are readily achieved in a number of transitions, particularly the higher J transitions of CO. In such cases the effective spontaneous emission rate is lowered by a factor of β, with a corresponding decrease in the critical density. The quantities shown are representative only, since β is highly dependent on the model chosen for kinetic temperature, density, and column density. But the general trend of decreasing β for higher J transitions is appropriate to a range of models representative of Sgr A West.

The transitions listed span about four orders of magnitude in critical density. The CO $J = 1$–0 transitions has the lowest critical density, expressing the well-known fact that CO emission traces out regions of low density molecular gas. The CO $J = 3$–2 transition traces gas of intermediate excitation, having a critical density more than an order of magnitude greater than the 1–0 transition and more than an order of magnitude less than the 7–6 transition.

b) Comparison with CO $J = 1$–0 Emission

The CO observations of this paper may be compared with a variety of observations of other rotational transitions of CO from this region. Earlier CO $J = 1$–0 observations covered on a fairly large scale the distribution of molecular material in the inner galaxy (Liszt *et al.* 1977; Bania 1977; Liszt and Burton 1978). These observations revealed a number of features of the molecular distribution, including the 3 kpc arm and the "expansion" features at -135 and 165 km s^{-1}. In general

these features of the molecular gas were in very good agreement with those of the atomic gas seen in H I (Burton and Liszt 1978). Many of these features of the large-scale distribution of CO are clearly evident in the $J = 3$–2 data but are not of great interest in studying the high-density central galactic region. More recently Liszt, Burton, and van der Hulst (1985) studied the $J = 1$–0 emission on a smaller scale and found that the high-velocity CO emission displayed a double-lobed structure similar to that seen from far-infrared dust emission.

Of greatest interest are the higher resolution observations of Serabyn *et al.* (1986). These observations revealed distributions very similar to those shown in Figure 2: emission dominated by material in rotation about the center at a distance of about 3 pc. Since these observations had the same spatial resolution ($\approx 20''$), the differences in the maps should be directly attributable to excitation. As shown in Table 1, the $J = 3$–2 transition has approximately 30 times the critical density (n_{cr2}) of $J = 1$–0. However, for parameters thought to be representative of the neutral disk, this is reduced somewhat by the effects of trapping since the $J = 3$–2 line has an optical depth of unity or greater. Given this range of critical densities, the agreement between the two sets of maps is remarkable. Clearly in both cases the vast majority of the gas contributing to the CO emission is at densities of 10^4 cm^{-3} or greater.

It is useful to compare these two sets of maps quite closely, as a number of interesting differences may be seen. In doing so it is important to keep in mind the fact that there are some differences which are simply artifacts of the presentation (e.g., Serabyn *et al.* suppress their lowest contour and we do not). In the velocity range $-120 < v_{lsr} < -110$ km s^{-1} the $J = 1$–0 map exhibits a single main peak at ($\delta l = -2'20''$, $\delta b = -1'$). At lower absolute velocities this peak moves in toward the center and eventually divides into two main maxima at approximately ($\delta l = -1'40''$, $\delta b = 0$) and ($\delta l = -1'20''$, $\delta b = -1'$). These two peaks dominate the appearance of the blueshifted lobe down to -60 km s^{-1}, although a number of other minor peaks and plateaus are present. This behavior is *not* reproduced in the $J = 3$–2 data. Instead, at the extreme velocities (≈ -120 km s^{-1}) there is some emission at the position of the $J = 1$–0 peak, but it is only a minor feature of the map, with the bulk of the $J = 3$–2 emission located much closer to the center and rather broadly distributed. At lower velocities this peak disappears and the strongest feature in the map is the peak at ($\delta l = -1'40''$, $\delta b = 0$), also seen in $J = 1$–0. The other strong 1–0 peak is not as clearly evident, the emission at $\delta b < 0$ being more of a diffuse "extension" rather than a clear peak. Also strongly evident in $J = 3$–2 but only weakly suggested in $J = 1$–0 is a peak at ($\delta l = -40''$, $\delta b = 0$), which appears as part of the apparent "ridge" at $\delta b = 0$. The absence of the ($\delta l = -2'20''$, $\delta b = -1'$) peak from the $J = 3$–2 data strongly suggests that this material, at a projected galactocentric radius of about 8 pc, has a density of only about 10^4 cm^{-3}. In contrast, densities at 3 pc inferred from CS approach 4×10^5 cm^{-3}. The general trend of the $J = 3$–2 emission being more concentrated toward the center clearly indicates increasing excitation in the inner regions of the disk. The excitation depends on temperature and line opacities as well as density. The relationship of these three parameters will be discussed in more detail in § IV*b*. Besides this excitation gradient, differences between the $J = 1$–0 and $J = 3$–2 maps are attributable to the clumpy nature of the nuclear disk and the effects of optical depth.

There are similar differences in the appearance of the redshifted lobe. In $J = 1$–0 the high-velocity peak ($110 < v_{lsr} < 120$) appears at ($\delta l = 1'$, $\delta b = 20''$) whereas in $J = 3$–2 the peak is closer to the center, approximately ($\delta l = 40''$, $\delta b = 10''$). In the velocity interval $90 < v_{lsr} < 110$ km s^{-1} this resolves into two peaks at approximately ($\delta l = 50''$, $\delta b = 30''$) and ($\delta l = -10''$, $\delta b = 20''$). The peaks have similar locations in the two transitions although in $J = 1$–0 the northern of the two is considerably more intense whereas in $J = 3$–2 the peaks are of similar intensity. At still lower velocities ($80 < v_{lsr} < 90$) the $J = 3$–2 map shows an additional extension toward negative δb which is not evident at all in $J = 1$–0. As with the blueshifted lobe the chief difference between the maps is a concentration in $J = 3$–2 toward smaller galactocentric radius, with some additional differences in the details of the distribution. Despite the different radii at which the two transitions peak, the extreme velocities observed are rather similar. For the two lobes combined there is evidence for only a slight falloff in velocity from 3 pc out to 8 pc.

The peak antenna temperatures in the $J = 1$–0 and $J = 3$–2 maps provide some interesting additional information about the northern and southern lobes. In general it is difficult to obtain reliable information from ratios of intensities of lines at widely varying frequencies, due to potential differences in calibration. However, in the present case we have maps of sizable regions in these two transitions, and it is possible to study *relative* changes in intensity ratios. For example, consider the peak of the redshifted lobe in $J = 1$–0 at the position ($\delta l = 1'$, $\delta b = 40''$) in the velocity interval $90 < v_{lsr} < 100$ km s^{-1}. At this position the ratio of main beam brightness temperatures for $J = 3$–2 relative to $J = 1$–0 is near unity, indicating a high optical depth in this region. Further to the southeast, for example at ($\delta l = 1'$, $\delta b = 0$), the ratio of $J = 3$–2 to $J = 1$–0 is much higher, indicating a partially optically thin region of high excitation. A similar analysis of the blueshifted lobe yields generally higher ratios of $J = 3$–2 to $J = 1$–0, indicating this region is less optically thick than the redshifted lobe. Within the blueshifted lobe the optical depth is lowest along the ridge at $\delta b = 0$ and highest in the region around ($\delta l = -1'40''$, $\delta b = -1'$).

Besides the blueshifted and redshifted lobes, both maps show extensive material not in simple rotation about the center. From -80 to -60 km s^{-1}, both maps show a spatially extended cloud in the upper left map quadrant, a region in which blueshifted velocities are prohibited by models of simple rotation. The appearance of this cloud in the two transitions is quite similar, including the apparent shift in cloud center with velocity. The $J = 3$–2 map reveals an additional, apparently compact cloud in the lower left quadrant at ($\delta l = 1'$, $\delta b = -1'$) extending in velocity from -100 to -60 km s^{-1}. This cloud does not appear in the $J = 1$–0 data since it is located in a region which was not mapped in those observations. A third compact cloud at ($\delta l = 0'$, $\delta b = 40''$) is seen in $J = 3$–2 just in the velocity range $-70 < v_{lsr} < -60$ km s^{-1}. It is also seen in the $J = 1$–0 data, but its appearance there is very much weaker. At lower absolute velocities both maps show portions of the spatially extensive "50 km s^{-1} cloud" which peaks to the east of the center and the "20 km s^{-1} cloud" located south of center. Other views of this material have been given by Liszt *et al.* (1983), and Liszt, Burton, and van der Hulst (1985).

c) *Comparison with* CO $J = 2$–1 *and* 7–6 *Emission*

In the $J = 2$–1 transition, a set of unpublished observations of Sgr A West were made by Lo *et al.* (1983). These observa-

tions agree with the present $J = 3$–2 data in all essential respects, although they suffer from a lower spatial resolution of approximately 30″. In particular the $J = 2$–1 data agree with the data of Figures 1 and 2 in general spectral shape, in intensities, and in the sizes and locations of the emission peaks associated with the high-velocity gas in the neutral disk. The $J = 2$–1 data also confirm the existence and appearance of the -90 km s^{-1} cloud centered at $\delta l = 1'$, $\delta b = -1'$ which was not covered by the $J = 1$–0 observations of Serabyn *et al.* (1986).

The CO $J = 7$–6 observations of Harris *et al.* (1985) covered only a few positions with relatively low resolution (32″) and sensitivity, but nevertheless are important because of the high critical density of the transition. A major observational difference between $J = 7$–6 and the lower J CO observations is that the $J = 7$–6 emission peaks considerably closer to the center. This is to be expected for a disk in which density increases toward the center and continues the pattern established with the $J = 3$–2 peaking at smaller radii than $J = 1$–0. The peak of the $J = 7$–6 line occurs at a projected radius of approximately 1.5 pc, similar to that seen in other high excitation lines such as HCN $J = 1$–0 (see § III*d* below). These high-excitation lines are thought to trace out the highest density regions of the neutral disk, regions just outside the inner ionized cavity. As shown in Table 1, the lower J CO transitions trace considerably lower density gas. Figure 2 shows that this gas extends out to considerably larger distances from the center.

Another significant difference between CO $J = 7$–6 and the lower J transitions is optical depth. The optical depth in the $J = 7$–6 transition can become quite significant, and this in turn may complicate the interpretation of the observed spatial distribution. As discussed in the comparison between the $J = 1$–0 and $J = 3$–2 transitions, the behavior of the peak antenna temperatures suggested significant optical depths in the $J = 3$–2 line in some parts of the disk. The $J = 7$–6 intensities provide important information about excitation and optical depth, although this is limited by the small number of positions observed. The majority of the $J = 7$–6 observations were offset from the center purely in Galactic longitude. This strip of positions misses the most intense part of the redshifted lobe, although it does manage to cover much of the intense ridge along the western edge of the blueshifted lobe. Where data are available the brightness temperatures in the $J = 7$–6 and $J = 3$–2 transitions are comparable, indicating high excitation and a significant opacity in the $J = 7$–6 line. The one exception is the innermost position in the blueshifted lobe ($\delta l = -30''$) which is clearly optically thin, at least in the lower J transitions.

Harris *et al.* (1985) conclude that the CO emission occurs in a region of density about 3×10^4 cm^{-3}, gas temperature of 300 K, and beam-averaged column density of 2×10^{18} cm^{-2}. These values are in good agreement with other determinations. They also agree that the $J = 7$–6 emission has a typical optical depth of $\tau \approx 1$. As to kinematics, they see an apparent decrease in velocity centroids and also terminal velocities as one moves out from the center. This apparent falloff does *not* agree with the behavior seen in either $J = 1$–0 or $J = 3$–2. Because of the considerably higher signal to noise ratios of the lower J observations, it seems likely that the disk rotational velocity does not fall off as rapidly as suggested by Harris *et al.* The authors also conclude from the large line widths seen that considerable random and large-scale noncircular motions are present. This is in good agreement with a wide range of other observations.

d) Comparison with Other Molecular Transitions

Various other molecular species have been observed toward the Galactic center including NH_3 and OH (Güsten, Walmsley, and Paul 1981; Serabyn and Güsten 1986; Genzel *et al.* 1985). Of greatest interest for our present purposes, because of the high spatial resolution, are the interferometric observations of HCN (Güsten *et al.* 1987). These observations have given the best view of the ringlike nature of the molecular material, with a sharp inner boundary at a radius of 2 pc, and with an essentially empty inner cavity. The ring is clumpy, with a strong peak near our position ($\delta l = -40''$, $\delta b = 0$) and with diminished intensity on the eastern side. In part this diminished intensity may be attributed to absorption by low-velocity foreground gas. The progression of velocities across the map is continuous, illustrating that the gas is part of a single, coherent, rotating structure.

In Figure 3 we have plotted a comparison between the HCN interferometer map and the current CO $J = 3$–2 data. The HCN contours are from the velocity-integrated maximum entropy method (MEM) map of Güsten *et al.* (1987). The field of view of the interferometry map is only about 3′.5 in δl, which may result in the suppression of some emission near the edges of the map. The CO $J = 3$–2 emission which has been plotted is from velocities near the maximum rotational velocity of the disk, in the range $110 \leq |v_{\rm lsr}| \leq 120$ km s^{-1}. For an inclined rotating disk, emission at high velocities highlights the extreme positions along the major axis of the disk. This effect is clearly seen in Figure 3. Comparison with lower velocity CO emission would show emission which filled out the minor axis portion of the disk structure. The correspondence between HCN and CO $J = 3$–2 is quite good, much better than that between HCN and CO $J = 1$–0 shown by Figure 3*c* of Güsten *et al.*, indicating in particular the way in which the $J = 3$–2 CO highlights the dense inner portions of the disk.

The redshifted (northern) lobe shows very close correspondence between HCN and CO $J = 3$–2. In both cases the emission is compact and located quite close to the nominal center. In the higher velocity channels shown in Figure 3 the CO cloud has a single peak and is roughly symmetrical. At lower velocities (e.g., $90 < v_{\rm lsr} < 100$ km s^{-1}) the CO emission divides into two peaks, which are in almost perfect correspondence with the peaks in the HCN map. The close correspondence between these tracers indicates that almost all the gas in this part of the disk is at quite high density.

The southern blueshifted lobe is considerably more complex. The HCN exhibits a single intense peak quite close to the center with additional diffuse emission out to much larger distances. This position is also a peak in CO $J = 3$–2 although there is considerable CO emission further out; indeed, the region of strongest CO emission is approximately twice as far out as the HCN peak. As opposed to the northern lobe, the southern lobe exhibits a considerable excitation gradient as one moves out in the disk. Such a gradient is also evident from the differences between the CO $J = 1$–0 and $J = 3$–2 lines with the $J = 1$–0 peak occurring at still larger distances.

A similar effect is seen from observations of high-J transitions of CS. Serabyn, Güsten, and Evans (1988) observed the $J = 2$–1, 3–2, and 5–4 transitions of CS from a variety of positions in the southern (blueshifted) lobe of the neutral disk. From the observed line ratios, they concluded the density varied by almost an order of magnitude, from about 4×10^5 cm^{-3} near the position of the main HCN peak down to about

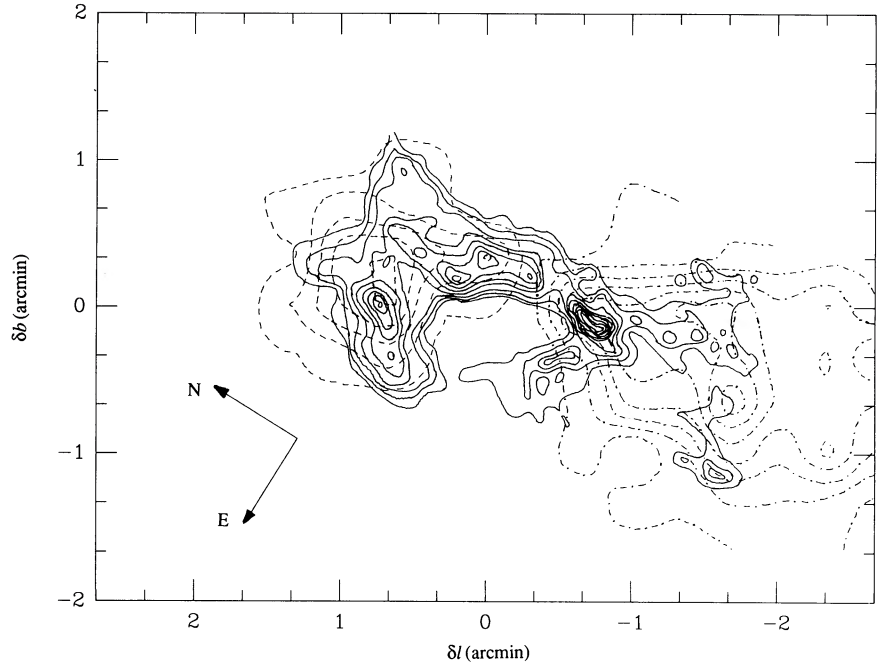

FIG. 3.—Comparison between velocity-integrated MEM map of HCN by Güsten *et al.* (1987) and CO $J = 3$–2 emission in the interval $110 \leq |v_{lsr}| \leq 120$ km s^{-1} (this work). The HCN contours are represented by solid lines, redshifted CO by dashed lines, and blueshifted CO by alternating dots and dashes.

5×10^4 cm^{-3} in the outer regions of the disk, about 7 pc from the center.

e) Comparison with Atomic Fine-Structure Lines

Also observed toward the Galactic center are fine-structure transitions of the atomic and ionic species C II, O I, and O III (Genzel *et al.* 1984, 1985; Lugten *et al.* 1986). The observations of the spatially extended O I emission indicated the predominantly neutral nature of the material in the inner disk. Requirements for collisional excitation suggested hydrogen densities of around 10^5 cm^{-3} and a gas temperature of around 300 K. The kinematic picture was of a rotating disk with nearly constant rotational velocity but with some substantial noncircular motions present. The generally weak O III emission tended to confirm the absence of lower density atomic gas. All of this is in good agreement with the picture derived from observations of the molecular gas.

Somewhat more controversial are the conclusions reached by Lugten *et al.* (1986) from their observations of C II. The C II emission is relatively easy to excite in lower density regions ($n \approx 10^3$ cm^{-3}) and thus it is seen to be spatially more extended than O I. Velocity centroids of C II were found to fall off with increasing distance from the center, suggesting a strong pointlike mass concentration and a near-Keplerian rotational velocity pattern. This is clearly not in agreement with the present CO $J = 3$–2 data nor with the $J = 1$–0 data of Serabyn *et al.* (1986). Both sets of CO data indicate rotation velocities of about 120 km s^{-1} persisting out to at least 7 pc from the center, whereas the C II data suggest a falloff to about 80 km s^{-1} over somewhat similar distances. Lugten *et al.* suggest as a possible explanation for this falloff a blending with emission from lower velocity clouds. It certainly seems difficult to reconcile these observations without invoking a substantially different volume of gas being sampled by the C II. A more complete discussion of the anomalous situation of the C II observations is contained in Güsten *et al.* (1987).

IV. DISCUSSION

a) Geometrical Structure of the Disk

There is by now considerable agreement as to the general physical structure of the circumnuclear disk, and this picture is largely supported by these CO $J = 3$–2 observations. The disk is thought to be a coherent structure in rotation about the Galactic center and to possess a fair degree of axial symmetry. The axis of the disk is inclined about 70° with respect to the line of sight, as determined from the ratio of major to minor axis extent. There seems to be a variation in the plane of the disk as a function of position (the disk is said to be "warped"), and the average position angle of the plane is distinctly different than that of the inner Galaxy as a whole. The disk is fairly thin, although its thickness seems to increase with distance from the center, an effect which is consistent with the degree of turbulent support expected in hydrostatic equilibrium. These geometrical properties of the disk are discussed more thoroughly by Güsten *et al.* (1987). Despite the fact that most investigators invoke axially symmetric disk models, it is clear that the circumnuclear material is not symmetrically distributed. There exists a clear north/south asymmetry which is seen quite markedly in these CO data. There is also an east/west (minor axis) asymmetry seen in the HCN interferometer map.

Observations of molecular and neutral atomic species and warm dust emission reveal a central hole in the disk. The HCN data show this inner edge to be rather sharp and to fall at a radius of about 1.7 pc. The inner cavity is largely empty, but contains a number of apparently infalling streamers of ionized gas. Some of the ionized gas, that associated with the "western arc," appears to be in nearly circular orbits and is probably the ionized inner boundary of the neutral disk. The gas in the northern and eastern arms seems to be in eccentric orbits (Serabyn and Lacy 1985; Serabyn *et al.* 1988). The velocities of these streamers at the positions where they touch the neutral disk are in good agreement with the velocities of the adjacent

molecular gas. This suggests the streamers may be caused by clouds of gas becoming detached from the nuclear disk, simultaneously falling toward the center and becoming ionized (Ekers *et al.* 1983; Lo and Claussen 1983).

The gas in the disk is clearly highly clumped. Three types of evidence support this. The first is the obviously highly irregular distribution of intensities in molecular maps such as our Figure 2 and the HCN map of Güsten *et al.* (1987). The resolution of the HCN map is high enough to permit a direct determination of clump size. Clumping is clearly present down to the resolution limit of 5″–10″ (0.25–0.5 pc). Obviously, smaller scale clumping may also exist. A second argument for clumping is provided by the apparent optical depth in CO. Since CO $J = 1$–2 and $J = 3$–2 antenna temperatures are rather similar, we have argued that the intermediate-J CO lines must have a reasonably high optical depth through the line-producing regions. The CO in these levels is nearly thermalized at temperatures of 100–200 K, as discussed below. However, observed CO main beam brightness temperatures are on the order of 20 K, suggesting that the CO is clumped with a beam-filling factor of about 0.1–0.2. A third argument is derived from the density of H_2 which from CS observations we know is about 10^5 cm^{-3}. If such gas filled the disk, then taking a typical line of sight through the disk to be 3 pc long and taking a ratio of CO to H_2 of 5×10^{-5}, one would derive a CO column density of 5×10^{19} cm^{-2}. This would be quite sufficient to make the CO optically thick and again one would conclude that the CO must be clumped. An important consequence of this clumping is the ability of UV radiation from the central region to penetrate out into the disk where it can be a significant heating source. These arguments also provide somewhat different information about the nature of the clumping. In particular, it is clear that clumping occurs across a range of densities. The CS and HCN observations could be satisfied by a model with a few regions with density 10^5 cm^{-3} or greater. The CO data, on the other hand, show that clumping is also present at the 10^4 cm^{-3} level and that the disk contains substantial regions of density lower than this.

b) Density, Temperature, and Column Density

Several sources of information have been used to determine global values of gas density and temperature in the neutral disk. Atomic fine-structure line observations have been used to derive a density of 10^5 cm^{-3} and a gas temperature of 300 K (Genzel *et al.* 1985). Observations of metastable NH_3 (Serabyn and Güsten 1986) have yielded a kinetic temperature of 240 ± 100 K, relatively independent of the gas density. Additional support for the high gas density has come from observations of high dipole moment species such as HCN and CS (Güsten *et al.* 1987; Serabyn, Güsten and Evans 1988), which have generally implied densities of a few times 10^5 cm^{-3} while being relatively insensitive to temperature. Estimates from CO $J = 7$–6 yielded a somewhat lower density of 3×10^4 cm^{-3}.

The CO $J = 3$–2 data provide considerable additional information about gas density, temperature, and CO column density. These observations may be used, in conjunction with the $J = 1$–0 data, to constrain the values of these parameters at a variety of specific locations throughout the neutral disk. The $J = 7$–6 data provide additional constraints, but only for the limited set of positions covered by those observations. The parameters of density, temperature, and column density are closely coupled. For example, the degree of excitation depends on the rate of collisions and therefore density, yet temperature is also important particularly for determining the rate of excitation to high-J levels. And column density, through photon trapping, also affects excitation; generally speaking, a large column density alleviates the need for a high physical density. All three parameters similarly enter into line opacities.

We have constructed a variety of models with different densities, temperatures, and column densities. These calculations are based on the procedures discussed in § III*a* and the Appendix, which we have extended to give line intensities and line ratios. We have also included temperature-dependent collision rates using a linear interpolation of downward rates derived from Schinke *et al.* (1985). The results of these calculations are shown in Figure 4 where we have presented line ratios of CO $J = 3$–2 to $J = 1$–0 and $J = 7$–6 to $J = 3$–2. Observed values for the $J = 3$–2 to $J = 1$–0 ratio range from near unity over the outer and central parts of the disk to values of 2–4 at selected positions on the inner portion of the disk. The observed $J = 7$–6 to $J = 3$–2 ratio is typically 0.9 over the rather limited range of positions available, except at the inner edge of the blueshifted lobe where it climbs to about 1.2.

These observations represent rather severe constraints on the column density of the clumps. The low observed antenna temperature ratio between $J = 3$–2 and $J = 1$–0 requires a high optical depth and high column density. For those portions of the disk where this ratio is near unity, the CO column density through a clump must be at least 2×10^{19} cm^{-3}. As

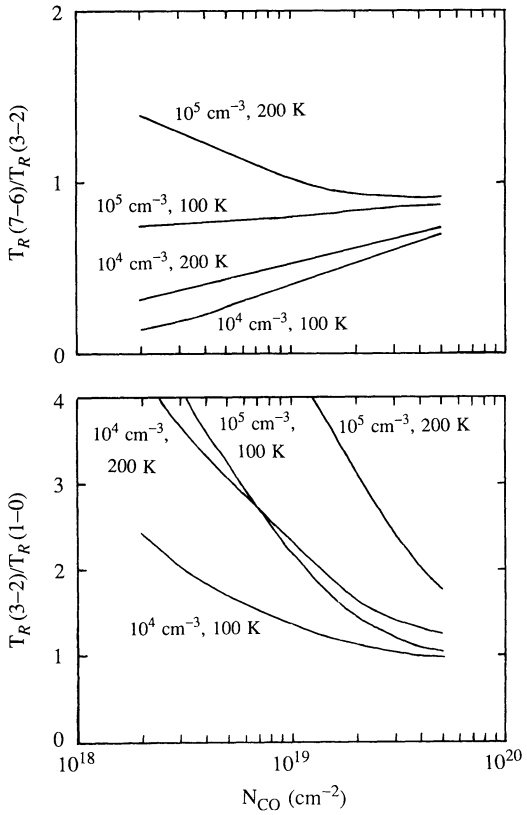

FIG. 4.—Calculated line temperature ratios for densities of 10^4 cm^{-3} and 10^5 cm^{-3}, temperatures of 100 K and 200 K, and a range of CO column densities. Column densities refer to a line of sight through an individual clump. For comparison, the observed $J = 3$–2 to $J = 1$–0 ratio ranges from near unity over the outer and central portions of the disk to values of 2–4 at the inner portion of the disk. The observed $J = 7$–6 to $J = 3$–2 ratio ranges from 0.9 to 1.2.

will be seen below, consideration of the CO/H_2 ratio indicates the CO column density is probably not much larger than this. In the inner regions of the disk where the $J = 3$–2 to $J = 1$–0 ratio is higher, the CO column density could be as low as about 2×10^{18} cm^{-2}, although the higher line ratio is probably partly due to temperature and density changes, as will be discussed below. The column densities derived above are based on the effects of opacity and refer to a line of sight through an individual clump. Corresponding beam-averaged column densities are roughly a factor of 5 smaller.

Physical density and temperature may be determined by considering the antenna temperature of the $J = 7$–6 line relative to $J = 3$–2. At the inner portions of the disk where this ratio is greater than unity one concludes the density must be about 2×10^5 cm^{-3} and the temperature about 200 K, although these parameters are strongly coupled. Similarly, farther out in the disk at a radius of 6 pc, the density drops to about 2×10^4 cm^{-3} and the temperature drops to about 100 K. These densities are in good agreement with the values inferred by Serabyn, Güsten, and Evans (1988) from CS. If the densities are held constrained to these values by the CS observations, then the temperature of 200 K for the inner disk and 100 K for the outer disk are reasonably well determined. These values are somewhat lower than the metastable NH_3 result of 240 ± 100 K. In our models, such lower temperatures are also helpful in reducing the calculated $J = 3$–2 to $J = 1$–0 ratio and thereby easing somewhat the requirement for large CO column densities.

A typical large, dense clump has a density of 10^5 cm^{-3} and a diameter of 0.5 pc, giving it a mass of 300 $M_\odot$. The column density of H_2 through such a clump is then 1.7×10^{23} cm^{-2}. Compared with an inferred CO column density of 2×10^{19} cm^{-2}, we get a CO/H_2 ratio of about 1.2×10^{-4} which, given the uncertainties of these estimates, is in good agreement with the typical value of 5×10^{-5} found for galactic molecular clouds. Clumps of this size are probably at the upper end of the range present in the disk. The total number of clumps present is on the order of 20–100. This is sufficiently few as to give some explanation for the clearly irregular distributions in the molecular maps. A summary of these physical properties of the neutral disk is contained in Table 2.

c) *Kinematics and Mass Distribution*

The general kinematic picture is clearly one in which the majority of the neutral gas appearing, in projection, within a few parsecs of the center is part of a coherent structure in rotation about the center. However, this pattern does not apply to all of the neutral gas, as there are a number of clouds with clearly noncircular velocities. Also there has been some disagreement as to the details describing the rotational motion of the disk. Both Harris *et al.* (1985) and Lugten *et al.* (1986) found evidence for a rotational velocity which dropped off with increasing distance from the center. This suggested a centrally peaked mass distribution, with most of the mass in the region located inside the 2 pc inner radius of the disk. Serabyn *et al.* (1986) with higher resolution mapping of CO $J = 1$–0 and also a more complete dynamical model concluded that the rotational velocity of ≈ 110 km s^{-1} was approximately independent of radius.

Our data clearly support the conclusion of Serabyn *et al.* that velocity is nearly independent of radius. Mostly, this conclusion is based on data from the southern, blueshifted lobe. In a qualitative sense it may be seen immediately from Figure 2. The map of $-130 < v_{lsr} < -120$ km s^{-1} clearly contains terminal velocities for large regions across the southern lobe ranging in radius from about 2 to 8 pc. More quantitatively one can construct a rotation curve by combining all the CO data. The innermost $J = 7$–6 spectrum gives a terminal velocity of -130 km s^{-1} from material presumably just outside the inner boundary of the disk, at an average radius of about 2 pc. Farther out in the disk one might look at the strong $J = 3$–2 peak at ($\delta l = -1'40''$, $\delta b = -40''$) with the same extreme velocity at 5.4 pc radius. The $J = 1$–0 data goes furthest from the center and may show a slight drop to -120 km s^{-1} at 7.6 pc. Looking at interclump regions gives much the same effect. The contrary conclusion of Harris *et al.* is undoubtedly related to their signal-to-noise ratio and the fact their data do not fall along the true major axis of the disk. As discussed earlier the observations of Lugten *et al.* are harder to reconcile, except perhaps by blending of the profiles with lower velocity material, as the authors suggest. We have followed previous workers in emphasizing the blueshifted lobe. In the redshifted lobe a similar pattern is present, with terminal velocities of about $+130$ km s^{-1} at 2 pc falling perhaps to 120 km s^{-1} at 3.2 pc. It is difficult to trace the rotation curve much further out into the red lobe simply for lack of emitting gas.

After allowing for a turbulent linewidth of 50 km s^{-1} and allowing for an inclination of 70°, one infers a rotational velocity of the disk of 110 km s^{-1}. This velocity field may be used to estimate the mass distribution by assuming circular rotation. As will be seen, the material undergoing clearly noncircular motions represents only a small fraction of the mass of the gas. At a radius of 2 pc the rotational velocity implies an enclosed mass of $M(2\text{ pc}) = 5.6 \times 10^6\ M_\odot$. Since the rotational velocity is roughly constant, the enclosed mass varies roughly linearly with radius as one moves out into the disk. In this picture the mass is less centrally concentrated than suggested by Lugten *et al.*, with a significant contribution from an extended stellar cluster. The inferred mass between 2 pc and 8 pc from the center is $1.5 \times 10^7\ M_\odot$, consistent with that derived from the 2 μm surface brightness distribution and an M/L ratio of 1 $M_\odot/L_\odot$ (cf. Genzel and Townes 1987). This of course does not rule out the possibility that within the inner radius of the disk the mass distribution is dominated by a central pointlike mass, as may be indicated by observations of high-velocity motions in the ionized gas.

There are a variety of indications of substantial noncircular gas motions. One is the observed turbulent line width, which

TABLE 2

PARAMETERS OF THE NEUTRAL DISK

Parameter	Value
Inclination	70°
Position angle of major axis	10°–30°
Temperature (range)	100–200 K
Density (range)	2×10^4–2×10^5 cm^{-3}
CO column density (clump)	2×10^{19} cm^{-2}
CO column density (beam average)	2×10^{18} cm^{-2}
Filling factor (area)	0.1–0.2
Filling factor (volume)	0.05
Clump mass (typical)	100 $M_\odot$
Turbulent velocity width	50 km s^{-1}
V_{rot} (2 pc)	110 km s^{-1}
V_{rot} (8 pc)	105 km s^{-1}
Enclosed mass within 2 pc	$5.6 \times 10^6\ M_\odot$

reflects both internal velocities within a clump and relative motions between clumps. The placement of the clumps and their relative velocities suggest a collisional time scale of 10^5 yr, comparable to the rotational period of the disk. Finally there are a variety of clouds, discussed previously in §§ II and III*b*, which are clearly not part of the rotating disk structure. Mass estimates based on intensity and spatial extent suggest that these clouds represent about 6% of the high-velocity CO in the region mapped. A critical issue is whether these objects are located at the Galactic center or are located some distance away, perhaps in the foreground. The fact that three of these objects have similar blueshifted velocities and could be associated may indicate the latter possibility. However, the excitation inferred for these clouds is rather high (particularly for the cloud with $v_{\rm lsr}$ between -70 and -60 km s^{-1} centered at $\delta l = 0'$, $\delta b = 40''$) which suggests they *are* near the center. Discounting these blueshifted clouds leaves only the redshifted cloud at ($\delta l = 0'$, $\delta b = 20''$) discussed by Serabyn *et al.*, which is too near the axis for its velocity to be explained by the rotation of the neutral disk. It also may not be physically located at the center, although its close association with the main part of the redshifted lobe both spatially and in velocity indicates it probably is near the center. In all, the uncertainties in the locations of these clouds makes it impractical to use their velocities to obtain significant additional information about the mass distribution.

V. SUMMARY

We have observed emission from the $J = 3$–2 rotational transition of CO over a substantial region in Sgr A West. The region mapped encompasses the dense rotating neutral disk, a structure which extends out to a radius of about 8 pc from the Galactic center. The resolution of 20″ is sufficient to reveal considerable structure within the disk. These observations show significant differences from previous CO $J = 1$–0 observations of Serabyn *et al.* (1986). In particular, the $J = 3$–2 emission is more centrally concentrated, and there are differences in the relative strengths of emission peaks in the two sets of maps. A larger region was mapped in $J = 3$–2, revealing additional material not in simple rotation about the center. In comparison with the CO $J = 7$–6 observations of Harris *et al.* (1985), the $J = 3$–2 emission is *less* centrally concentrated. There is quite good agreement between features of the $J = 3$–2 maps and the HCN $J = 1$–0 interferometric map of Güsten *et al.* (1987). The agreement is much closer than that between the HCN and the CO $J = 1$–0.

The picture derived is one of a disk with a significant excitation gradient, since the emission from high-excitation species declines as one moves out from the center. Typical values of the physical conditions present are density $n = 2 \times 10^4$–2×10^5 cm^{-3} and temperature $T = 100$–200 K. The gas in the disk is highly clumped. Antenna temperatures in the $J = 3$–2 and $J = 1$–0 transitions are quite similar, indicating optical depths greater than unity. Future observations of isotopic CO lines could yield important additional information about excitation. We infer a column density of CO along a line of sight through a clump to be $N_{\rm CO}({\rm clump}) \approx 2 \times 10^{19}$ cm^{-2}. The clumps range up to about 0.5 pc in size and have masses ranging up to a few hundred solar masses. The rotation curve is seen to be flat from 2 pc out to 8 pc, in agreement with the work of Serabyn *et al.* but contrary to the conclusions of Harris *et al.* (1985) and Lugten *et al.* (1986). The mass within the central 2 pc radius is $5.6 \times 10^6\ M_\odot$ and is less centrally peaked than suggested by Lugten *et al.*

This work has been supported in part by the National Science Foundation under grants AST-8715295 and AST-8818327. One of the authors (W. C. D.) acknowledges partial support from the L. W. Frohlich Research Fellowship of the New York Academy of Sciences. The authors are grateful to T. G. Phillips and the staff of the Caltech Submillimeter Observatory for their hospitality. Research at the CSO is supported by NSF grants AST-8311849 and AST-8815132.

APPENDIX

MOLECULAR EXCITATION

For a linear molecule the spontaneous emission rate is given by

$$A_{J,J-1} = \frac{64\pi^4}{3h}\frac{\nu^3}{c^3}\mu^2\frac{J}{2J+1}.$$

In calculating values for A-coefficients we have adopted permament dipole moments of 0.110 D for CO, 1.957 D for CS, and 2.984 D for HCN. Collisional excitation rates are based first on calculations of the potential energy surface of the molecular interaction. The dynamics of the scattering process are then calculated to give an average over orientations and over a thermal distribution of relative velocities. For consistency all collision rates will be given for a kinetic temperature of 100 K and an assumed collision partner of para-H_2. For CS the collision rates are taken from Green and Chapman (1978). For HCN we have started with rates from Green and Thaddeus (1974), in which the assumed collision partner is He, and have scaled the rates upward by a factor of 1.5 to approximate the effect of H_2 collisions. For CO the best available rates are those given by Schinke *et al.* (1985) based on the coupled-states approximation (their Table 4). Following Viscuso and Chernoff (1988) we have taken the 100 K rates of Schinke *et al.* and converted upward rates γ_{0J} to doward rates by application of detailed balance:

$$\gamma_{J0}(2J+1) = \gamma_{0J}e^{+\Delta E/kT}.$$

The downward rates into the ground state were then expanded into a matrix of downward rates (Goldflam, Green, and Kouri 1977) in the usual way:

$$\gamma_{JJ'} = (2J'+1)\sum_L (2L+1)\begin{pmatrix} J & L & J' \\ 0 & 0 & 0 \end{pmatrix}^2 \gamma_{L0}, \qquad J > J'$$

with the remaining upward rates determined again from detailed balance

$$\gamma_{J'J}(2J' + 1) = \gamma_{JJ'}(2J + 1)e^{-\Delta E/kT} .$$

The resulting rates are a slight refinement of the rates given by McKee *et al.* (1982). For the purposes of these calculations the differences are insignificant. The collision rates described above, together with the spontaneous emission rates, may be used to calculate either detailed populations of the individual levels, or the somewhat qualitative critical densities shown in Table 1.

The equilibration process described so far assumes that all emitted photons escape the cloud. In practice molecular clouds can have significant optical depths and this, in turn, can radically affect the equilibration of the molecular levels. The transition $J \rightarrow J - 1$ has an optical depth

$$\tau_{J,J-1} = \frac{c^3}{\nu^3}\frac{1}{8\pi}A_{J,J-1}\frac{1}{\Delta V}\left[N_{J-1}\frac{(2J+1)}{(2J-1)} - N_J\right],$$

where ΔV is the velocity line width of the emission, and this optical depth represents an average over the line profile. N_J and N_{J-1} are column densities of the rotational levels J and $J - 1$. The effect of this optical depth is geometry dependent. In the large velocity gradient formalism, it is customary to express the likelihood that an emitted photon escapes the cloud by the probability β, which for a spherical cloud with a velocity profile proportional to radius, is of the form

$$\beta = \frac{1 - e^{-\tau}}{\tau} .$$

An escape probability less than unity represents, in effect, a reduction of the spontaneous emission rate. Since the populations of the levels depend on the values of the β's and the β's depend on the populations, it is necessary to reach a self-consistent solution for these quantities.

REFERENCES

Bania, T. M. 1977, *Ap. J.*, **216**, 381.
Becklin, E. E., Gatley, I., and Werner, M. W. 1982, *Ap. J.*, **258**, 135.
Brown, R. L., and Liszt, H. S. 1984, *Ann. Rev. Astr. Ap.*, **22**, 223.
Burton, W. B., and Liszt, H. S. 1978, *Ap. J.*, **225**, 815.
Ekers, R. D., van Gorkom, J. H., Schwarz, U. J., and Goss, W. M. 1983, *Astr. Ap.*, **122**, 143.
Genzel, R., and Townes, C. H. 1987, *Ann. Rev. Astr. Ap.*, **25**, 377.
Genzel, R., Watson, D. M., Crawford, M. K., and Townes, C. H. 1985, *Ap. J.*, **297**, 766.
Genzel, R., Watson, D. M., Townes, C. H., Dinerstein, H. L., Hollenbach, D., Lester, D. F., Werner, M., and Storey, J. W. V. 1984, *Ap. J.*, **276**, 551.
Goldflam, R., Green, S., and Kouri, D. J. 1977, *J. Chem. Phys.*, **67**, 4149.
Green, S., and Chapman, S. 1978, *Ap. J. Suppl.*, **37**, 169.
Green, S., and Thaddeus, P. 1974, *Ap. J.*, **191**, 653.
Güsten, R., Genzel, R., Wright, M. C. H., Jaffe, D. T., Stutzki, J., and Harris, A. I. 1987, *Ap. J.*, **318**, 124.
Güsten, R., Walmsley, C. M., and Pauls, T. 1981, *Astr. Ap.*, **103**, 197.
Harris, A. I., Jaffe, D. T., Silber, M., and Genzel, R. 1985, *Ap. J. (Letters)*, **294**, L93.
Hollenbach, D., and McKee, C. F. 1979, *Ap. J. Suppl.*, **41**, 555.
Liszt, H. S., and Burton, W. B. 1978, *Ap. J.*, **226**, 790.
———. 1980, *Ap. J.*, **236**, 779.
Liszt, H. S., Burton, W. B., Sanders, R. H., and Scoville, N. Z. 1977, *Ap. J.*, **213**, 38.
Liszt, H. S., Burton, W. B., and van der Hulst, J. M. 1985, *Astr. Ap.*, **142**, 237.
Liszt, H. S., van der Hulst, J. M., Burton, W. B., and Ondrechen, M. P. 1983, *Astr. Ap.*, **126**, 341.
Lo, K-Y., and Claussen, M. J. 1983, *Nature*, **306**, 647.
Lo, K-Y., Sutton, E. C., Masson, C. R., Phillips, T. G., and Sargent, A. I. 1983, unpublished.
Lugten, J. B., Genzel, R., Crawford, M. K., and Townes, C. H. 1986, *Ap. J.*, **306**, 691.
McKee, C. F., Storey, J. W. V., Watson, D. M., and Green, S. 1982, *Ap. J.*, **259**, 647.
Oort, J. H. 1977, *Ann. Rev. Astr. Ap.*, **15**, 295.
Schinke, R., Engel, V., Buck, U., Meyer, H., and Diercksen, G. H. F. 1985, *Ap. J.*, **299**, 939.
Serabyn, E., and Güsten, R. 1986, *Astr. Ap.*, **161**, 334.
Serabyn, E., Güsten, R., and Evans, N. J. 1988, in *IAU Symposium 136, The Galactic Center*, ed. M. Morris (Dordrecht: Kluwer), in press.
Serabyn, E., Güsten, R., Walmsley, C. M., Wink, J. E., and Zylka, R. 1986, *Astr. Ap.*, **169**, 85.
Serabyn, E., and Lacy, J. H. 1985, *Ap. J.*, **293**, 445.
Serabyn, E., Lacy, J. H., Townes, C. H., and Bharat, R. 1988, *Ap. J.*, **326**, 171.
Sutton, E. C., Danchi, W. C., Jaminet, P. A., and Ono, R. H. 1989, *IEEE Trans. Microwave Theory Tech.*, submitted.
Viscuso, P. J., and Chernoff, D. F. 1988, *Ap. J.*, **327**, 364.
Wright, M. C. H., Marr, J. M., and Backer, D. C. 1988, in *IAU Symposium 136, The Galactic Center*, ed. M. Morris (Dordrecht: Kluwer), in press.
Yusef-Zadeh, F., Morris, M., and Chance, D. 1984, *Nature*, **310**, 557.

W. C. DANCHI, P. A. JAMINET, and E. C. SUTTON: Space Sciences Laboratory, University of California, Berkeley, CA 94720

C. R. MASSON: Center for Astrophysics, 60 Garden Street, Cambridge, MA 02138